Distribution of stress in Descending Plate in Special reference to Intermediate and Deep Focus Earthquakes ?. Characteristics of Thermal Stress Distribution

Tôhoku Geophys. Journ. (Sci. Rep. Tôhoku Univ. Ser. 5), Vol. 29, No. 2, pp. 81–105, 1983

Distribution of Stress in Descending Plate in Special Reference to Intermediate and Deep Focus Earthquakes

I. Characteristics of Thermal Stress Distribution

KAZUHIKO GOTO, HIROYUKI HAMAGUCHI and ZIRO SUZUKI

Geophysical Institute, Faculty of Science,
Tôhoku University, Sendai 980

(Received Sept, 14, 1982)

Abstract: Since locations and focal mechanism solutions of intermediate and deep focus earthquakes have been accurately determined, the focus of interest has been put on the relationship between seismic activity and tectonic process in descending plate beneath island arc. This series of studies intends to make a comprehensive study of this problem. As the first step of it, the present paper discusses the characteristics of thermal stress distribution in and around descending plate. The stress is estimated by FEM for various models. Physical parameters such as viscosity and thermal expansion coefficient are assumed to depend on pressure and temperature. Shear heating along the upper boundary between plate and asthenosphere is also taken into account.

The computation confirms that thermal stress distribution within plate is characterized by compressional and tensional stresses in upper and central parts of plate respectively, principal axes being almost parallel to dip direction. The magnitude of maximum shear stress, which relates to earthquake occurrence, depends strongly on convergence velocity and dip angle and it reaches up to 8 and 3 kbars in compressional and tensional fields respectively, when plate descends with convergence velocity of 8 cm/yr and dip angle of 45°. The calculation also indicates that the boundary condition at the bottom tip of plate and rate of shear heating are essential factors controlling the stress distribution.

1. General introduction

The first conceptional proposal on earthquake generating stress in descending plate was made by Isacks and Molnar (1971). The quantitative evaluation according to their idea was performed by several authors (Smith and Toksöz, 1972; Toksöz *et al.*, 1973; Sleep, 1975; Neugebauer and Breitmayer, 1975) and their results indicate that the stress distribution in descending plate is characterized by tension in shallow part and compression in deep part, if the descending is deep enough, say about 600 km. Recently, however, it has been established that the intermediate seismic zone is composed of two planes beneath some island arcs (e.g. Tsumura, 1973; Veith, 1974; Umino and Hasegawa, 1975). For an example, Umino and Hasegawa (1975) and Hasegawa *et al.* (1978a) clearly showed that the intermediate-depth earthquakes beneath Northeastern Honshu, Japan occur exclusively in two thin planes which are parallel to each other with distance of 30~40 km. The focal mechanism solutions derived from earthquakes

in upper plane are reverse faulting or down-dip compression, whereas those for earthquakes in lower plane are down-dip extension. Hasegawa *et al.* (1978b) also revealed that the upper seismic plane exactly coincides with the upper boundary of descending plate inferred from the difference in arrival times of ScS and ScSp, which is P wave converted from ScS at the boundary. These facts require a mutation of Isacks and Molnar's concept on stress field in descending plate.

Similar features of double-planed seismic zone have been reported for Kanto (Tsumura, 1973; Kasahara *et al.*, 1979; Suzuki *et al.*, 1980; Tsumura and Karakama, 1981) and Hokkaido (Suzuki and Motoya, 1981), as well as Kurile (Veith, 1974), Aleutian (Engdahl and Scholz, 1977), Alaska (Reyners and Coles, 1982) and Mariana (Samowitz and Forsyth, 1981). On the other hand, no report on the existence of double-planed seismic zone has been published, for examples, for Tonga (Billington, 1980) and New Hebrides (Pascal *et al.* 1978), even when the joint hypocenter determination and master event technique, which are thought to give sufficient resolution to disclose a double-planed feature, were adopted.

Several interpretations, such as those based on phase change of lithospheric materials, bending and unbending process, sagging of plate and thermal stress, have been presented in these years. Veith (1974) stated that the most probable cause of double-planed seismic zones may be the phase change from olivine to spinel, but no quantitative estimation of stress due to this cause was made in his paper. The stress due to bending and unbending has been proposed as the cause of double-planed structure of seismic zone (Engdahl and Scholz, 1977; Linde and Sacks, 1978; Tsukahara, 1980; Samowitz and Forsyth, 1981). The plate submerged with a constant dip angle after it is flexured downward at the trench. This implies the plate should be unbended so as to keep a flat plane shape subducting with a constant dip angle. The sum of stresses due to bending and unbending gives the elastic zone at the center of plate. Based on this idea, Engdahl and Scholz (1977) stated that earthquakes may occur around the edge of elastic zone. However, the yield strain as large as 3%, which corresponds to about 30 kbars in stress, is necessary to explain the distance between the upper and lower seismic zones. This magnitude of about 30 kbars is close to, or may even exceed, the fracture strength of the entire plate as noted by Sleep (1979). Sleep (1979) discussed the effect of sagging of plate and estimated the stress in and around plate quantitatively. According to his idea, asthenosphere provides little to accerelate or resist the plate subduction and the plate in its upper part is supported by oceanic lithosphere and in lower part by the friction between more viscous mesosphere. Sleep's calculation resulted that if a yield stress of about 200 bars is adopted, almost all regions in plate should be yielded. This result implies earthquakes occur in the entire plate, which disagrees with the location of double-planed seismic zone. Hamaguchi *et al.* (1977), Goto and Hamaguchi (1983) and Hamaguchi *et al.* (1983) presented the other cause of double-planed seismic zone. The colder lithospheric plate must be heated up in the hotter asthenosphere as it submerges and a non-uniform temperature distribution in the descending plate produces thermal stress in it. Their opinion is

that this thermal stress is responsible to earthquake generation. Hamaguchi *et al.* (1983) concluded, based on the quantitative considerations of thermal stress in a simple shape of plate, that thermal stress distribution can explain all characteristics of double-planed seismic zone mentioned above. Similar reports on thermal stress were also presented by Yang *et al.* (1977) and House and Jacob (1982).

Generally speaking, all of the four factors mentioned above are related to the earthquake generating stress within descending plate. However, most studies so far treated effect of each factor separately, and the models adopted by authors are different from each other. In some cases, only a qualitative result was given. Furthermore, above studies described only the explanation of double-planed structure of intermediate seismic zone and stated none of the relationship with occurrences of deep earthquakes. As mentioned by Elsasser (1969), the stress generating intermediate events should be related to those for deep ones, if the subduction of plate plays an essential role of stress guide for earthquake occurrence. The revised concept for stress within the whole plate shoule be so as to be able to explain the seismicity patterns not only of intermediate but also deep focus earthquakes.

Under the present situation of study, the main purpose of this series of studies is to present a new concept on comprehensive stress distribution in descending plate. As the first step, the present paper discusses the distribution of thermal stress in and around plate, and the comparison with stresses due to other causes and the relation of total stress and seismicity will be described in the following papers.

2. Description of model and method

The basic scheme of computation is as follows: Oceanic plate of 80 km in thickness, which has traveled horizontally above oceanic asthenosphere, begins to submerge into asthenosphere at a point corresponding to the location of trench shown by solid reverse triangle in Fig. 1. The plate bends continuously with a downward concave curvature until the subduction becomes to be a constant dip angle Θ and a constant velocity Vc. The idea is schematically illustrated in Fig. 1. Taking the beginning

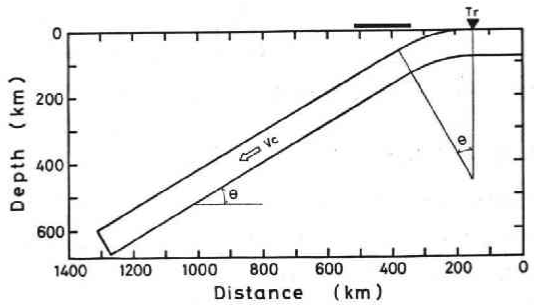

Fig. 1. Schematic representation of the descending plate of convergence velocity Vc and dip angle Θ. Solid triangle and thick solid line indicated at the upper of this figure are the positions of the trench axis and land area respectively.

time of submersion as a starting point, calculation is made at every time stage with a step of 80 km/Vc until the bottom tip reaches approximately 600 km in depth. The final stage is considered to correspond to the present status, on which the occurrence of recent earthquakes may reflect. The numerical computation is made for every combination of θ=30, 45 and 60° and Vc=2, 4 and 8 cm/yr.

In this series of papers the finite element method (FEM) is used to evaluate temperature and stress, because the equations of heat conduction and elasticity are difficult to be solved analytically under arbitrary initial and boundary conditions. Since adopted method and model give considerable influence on result, it is necessary to describe rather in detail the shape of model, dependency of physical properties on temperature and pressure and scheme of numerical computation.

2.1. *Shape of plate*

The upper boundary of descending plate has been established to coincide with the upper sheet of the double-planed intermediate seismic zone by travel time studies of ScS and ScSp, which is the converted wave of ScS at the plate boundary, from deep-focus earthquakes (e.g. Okada, 1971; Hasegawa *et al.*, 1978b). No clear observational evidence has been found about the location of lower boundary of descending plate. Many authors investigated the thickness of oceanic lithosphere and most of them scattered in the range of 50 to 100 km (e.g. McKenzie, 1967; Yoshii, 1973). Therefore it may be reasonable that the thickness of lithospheric plate is fixed to be 80 km in this study.

The bending of plate after beginning of submersion is thought to have a constant curvature until dip angle reaches a specified value of θ (see Fig. 1). The radius of curvature at upper boundary of plate is assumed to be 460, 295 and 215 km for θ=30, 45 and 60° respectively, referring to seismicity pattern in subduction zone. In the bending part, the linear velocity V of subduction at arbitrary point within plate is taken to be $Vc \times r/r_0$, where r and r_0 are radii of curvature at that point and center of plate respectively so that the same number of elements in FEM calculation is included in one step of iteration. For example, the velocity is 8.76 cm/yr and 7.24 cm/yr at upper and lower surface of bending plate when Vc=8 cm/yr and θ=30°. Below the bending part, plate has a rectangular shape with a constant dip angle of θ and subducts with a constant velocity Vc. The length of this straight subduction part are 1000, 760 and 540 km for θ=30, 45 and 60° respectively.

2.2. *Scheme of numerical computation*

As mentioned before, the present calculation takes an iterative procedure repeated successively for each time stage starting at the time of beginning of plate subduction. In each stage the distribution of temperature in and around plate is first calculated and then the stress distribution is estimated based on the temperature distribution. Two dimensional FEM is adopted assuming the state of plane strain.

The temperature distribution in and around the descending plate can be obtained

by solving the constitutive equation,

$$\boldsymbol{W} = \boldsymbol{V} \cdot \delta \boldsymbol{T} , \tag{1}$$

where $\boldsymbol{W}$ denotes the heat source in the concerned region and $\delta \boldsymbol{T}$ stands for an increment of temperature. $\boldsymbol{V}$ is a known matrix connecting $\boldsymbol{W}$ and $\delta \boldsymbol{T}$ and it contains such parameters as density, thermal conductivity and specific heat at constant pressure. The detailed explanation on adopted values of these factors will be made in the next section.

The thermal stress due to temperature distribution in a visco-elastic body can be estimated according to Horii and Kawahara (1970). The equation including visco-elastic and thermal effects is written as

$$\boldsymbol{F} = \boldsymbol{K} \cdot \delta \boldsymbol{u} - \boldsymbol{G} \cdot \{\alpha \boldsymbol{T}\} - \boldsymbol{H} \cdot \{\sigma(0)\} , \tag{2}$$

where $\boldsymbol{F}$ is body force, $\delta \boldsymbol{u}$ displacement from former stage, α coefficient of linear thermal expansion and $\sigma(0)$ stress in former stress stage in iterative calculation. Matrices of $\boldsymbol{K}$, $\boldsymbol{G}$ and $\boldsymbol{H}$ connect body force and displacement, temperature and stress respectively. Among them $\boldsymbol{K}$ is sometimes called stiffness matrix. Since $\boldsymbol{F}$, $\boldsymbol{K}$, $\boldsymbol{G}$, α, $\boldsymbol{T}$, $\boldsymbol{H}$ and $\sigma(0)$ are known for former stage, the increment of displacement $\delta \boldsymbol{u}$ can be obtained by solving eq. (2) and stress distribution is estimated using stress-strain relationship in a visco-elastic body. Although some subsidiary variables are originally used in eq. (2), they are eliminated eventually in the final calculation of stress. The flow-chart of algorithm is seen in Fig. 2.

The area where the computation is made is represented in Fig. 3. Asthenosphere areas of 195 and 165 km in thickness are taken into consideration above and below descending plate whose thickness is fixed to be 80 km. Beyond the bottom tip of plate the area of 120 km in dip direction is also considered. The computation is carried out also for 140 km in distance toward ocean from trench (solid revearse triangle in Fig. 3) where subduction starts.

The constitution of elements in FEM is shown in Fig. 3. As seen in this figure, all elements except for bending portion of plate are of shape of right angled triangle, of which the dimensions within plate are 20 km and 10 km in dip direction and perpendicular to it respectively. In asthenosphere the shape of element is also right angled triangle, which are parallel to those within plate, but its size increases as it goes apart from the boundary between asthenosphere and plate. The total number of elements are 3432, 2640 and 2464, corresponding to mesh point numbers of 1817, 1403 and 1311, in cases of $\Theta = 30$, 45 and 60° respectively.

The geothermal distribution by Von Herzen (1967) is adopted as the initial conditon at starting stage of computation. The mechanical boundary conditions of free stress and displacement are taken at circumference of area in concern. Although no mechanical boundary condition is explicitly adopted at the boundary between lithosphere and asthenosphere, it implies that displacement and stress are continuous. In most cases, the conditions of free displacement and stress are also assumed at the bottom tip of plate.

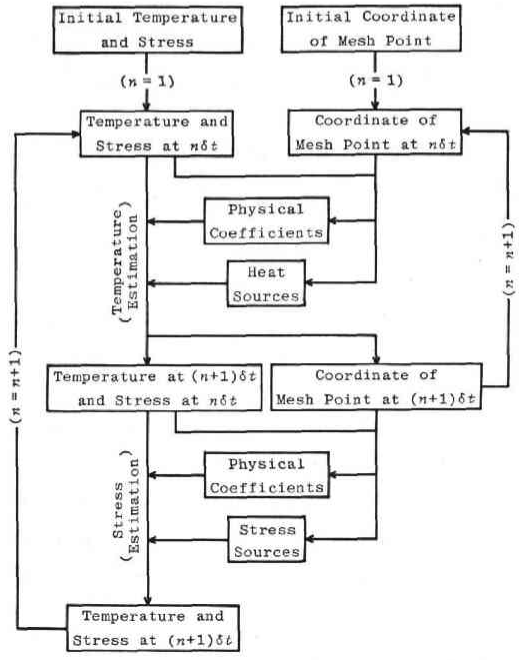

Fig. 2. Block diagram of the present calculation.

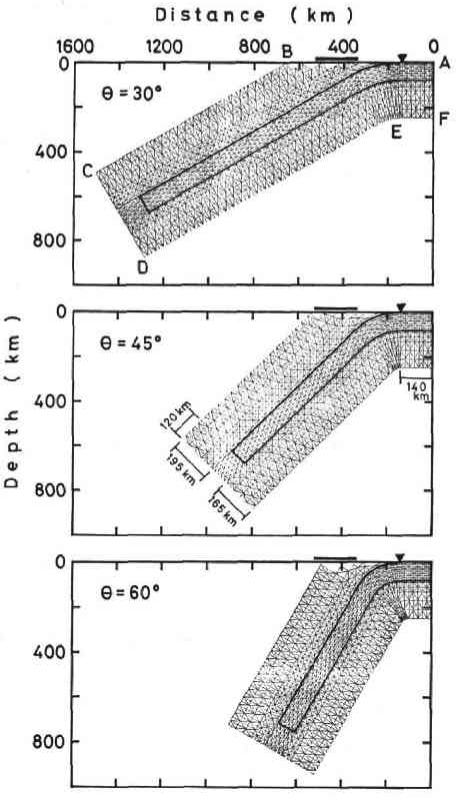

Fig. 3. Constitution of element in FEM. The portion surrounded by thick solid line represents the descending plate.

As thermal condition, two hear source are taken into account. One is a constant shear heating of 1.5×10^{-11} cal/cm^3·sec in a very thin layer (2.5 km in thickness) over the upper boundary of subducting part of plate, the value being taken from Minear and Toksöz (1970). Another heat source is due to the phase change from olivine to spinel, on which the discussion will be made in the next section. Many authors (e.g. Ringwood, 1970) have estimated the energy release due to this phase change. Taking a rough average of their results, heat source of 1.8×10^{-14} cal/cm^3·sec is given at the elements where the transition occurs in the present study.

2.3. *Physical properties*

Various physical properties and their dependency on temperature and pressure for litho- and astheno-spheric materials have to be taken into account in assessing temperature and stress distributions in and around descending plate.

The density at high temperature and high pressure is expressed by the Birch-Mürnaghan equation of

$$P=\frac{3}{2}K(T,0)\times(x^7-x^5)\times\left\{1+\frac{3}{4}(m-4)\times(x^2-1)\right\}, \tag{3}$$

where

$$x=\left\{\frac{\rho(T,P)}{\rho(T,0)}\right\}^{1/3},$$

and (4)

$$m=\frac{\partial K(T,0)}{\partial P}.$$

$K(T, P)$ and $\rho(T, P)$ denote bulk modulus and density at temperature T and pressure P. $K(T, P)$ and $\rho(T, 0)$ in eqs. (3) and (4) are represented as

$$K(T,P)=K(0,0)\exp\left\{-\delta\int_0^T\beta(T,0)dT\right\}\times\left\{\frac{\partial K(T,P)}{\partial P}\right\}_T\times P, \tag{5}$$

and

$$\rho(T,0)=\rho(0,0)\times\left\{1-\int_0^T\beta(T,0)dT\right\}, \tag{6}$$

where β is volumetric thermal expansion coefficient and δ is the Grüneisen-Anderson parameter, of which the value is fixed to be 5 throughout the present calculation according to Sawamoto (1977). The dependency of β, as well as shear modulus μ, on T and P is given by

$$\beta(T,P)=-\frac{1}{\rho(T,P)}\times\left\{\frac{\partial\rho(T,P)}{\partial T}\right\}_P, \tag{7}$$

and

$$\mu(T,P)=\mu(0,0)+\left\{\frac{\partial\mu(T,P)}{\partial P}\right\}_T\times P+\left\{\frac{\partial\mu(T,P)}{\partial T}\right\}_P\times T. \tag{8}$$

Therefore K, μ, ρ and β at T and P can be estimated, if $\beta(T,0)$, $\rho(0,0)$, $K(0,0)$, $\mu(0,0)$, $\{\partial K(T,P)/\partial P\}_T$, $\{\partial\mu(T,P)/\partial T\}_P$, $\{\partial\mu(T,P)/\partial P\}_T$ and δ are known.

Table 1. Elastic properties of olivine and spinel

Elastic Parameter	Structure	
	Olivine	Spinel
$\rho(0,0)$	3.330 gr/cm^3	3.683 gr/cm^3
$K(0,0)$	1.274×10^{12} dyne/cm^2	1.87×10^{12} dyne/cm^2
$\mu(0,0)$	7.72×10^{11} dyne/cm^2	1.08×10^{12} dyne/cm^2
$\{\partial K(T,P)/\partial P\}_T$	5.13	4.5
$\{\partial\mu(T,P)/\partial P\}_T$	1.80	0.612*
$\{\partial\mu(T,P)/\partial T\}_P$	-1.2×10^8 dyne/cm$^2\cdot$°K	-8.5×10^7 dyne/cm$^2\cdot$°K*

* Data denoted by * are from Sawamoto (1977) and the other data are from Chung (1971).

Since the olivine-spinel phase change is taken into consideration in the present calculation, as explained later, every quality should be assumed for both olivine and spinel. The numerical value of $\beta(T, 0)$ is taken from Suzuki's (1975, 1980) paper. Other qualities are assumed as in Table 1 based on studies by Chung (1971) and Sawamoto (1977) for olivine and spinel.

Using the estimated values of $\beta(T, P)$, $K(T, P)$ and $\rho(T, P)$, the specific heat at constant pressure, C_p, can be calculated by the equation

$$C_p(T, P) = \frac{\beta(T, P) \times K(T, P)}{\gamma \times \rho(T, P)}, \tag{9}$$

where γ is Grüneisen constant. The value of γ is fixed to be 1.20 for both olivine and spinel according to Sumino *et al.* (1977).

The thermal conductivity is given by the sum of lattice (phonon), radiative and exciton conductivities, among which the first one is most predominant at low temperature (Lubimova, 1967). The formulation of radiative and exciton conductivities as well as numerical values of constants, was given by Lubimova (1967) and Iriyama (1966). Since the value of a constant in the expression of lattice conductivity was not given in these papers, the experimental result by Kingery *et al.* (1954) on thermal conductivity of Mg_2SiO_4 (olivine) at 100°C, where the conductivity is mostly due to lattice conductivity. The numerical value of the constant κ_0 is obtained as 8.724×10^{-20} c.g.s. from this experiment. Consequently the value of thermal conductivity can be estimated at an arbitrary temperature and pressure.

Ringwood (1970) suggested that olivine occupies 57% in weight in his pyrolite model for mantle material. For simplicity, the material of litho- and astheno- spheres is assumed to be magnesium-rich olivine in this study. Then the phase change from olivine to spinel should occur in some portion of concerned area in calculation. Ringwood (1972) and Akimoto *et al.* (1976) showed that the temperature and pressure slope in phase diagram is about 30°C/kbar in all range of temperature. Recently, however, Sung and Burns (1976) stated that, when the dynamic effect is taken into account, the phase change is vertually zero below 700°C no matter how the metastability of material is. The difference between these two ideas does not cause so essential influence in stress field as far as the stress field due to temperature distribution is concerned, although the stress distribution due to phase change is strongly dependent on the difference in phase diagram as mentioned by Goto *et al.* (1983).

When the two phases of olivine and spinel exist jointly, the physical properties of material are estimated by the combination of those for two phases. For an example, the density $\rho(T, P)$ is given by

$$\rho(T, P) = B(T, P) \times \rho_{ol}(T, P) + \{1 - B(T, P)\} \times \rho_{sp}(T, P), \tag{10}$$

where ρ_{ol} and ρ_{sp} are densities for olivine and spinel and $B(T, P)$ is the proportion of olivine at T and P, the value changing from 0 to 1.

The variations of physical constants thus estimated are shown in Fig. 4 against

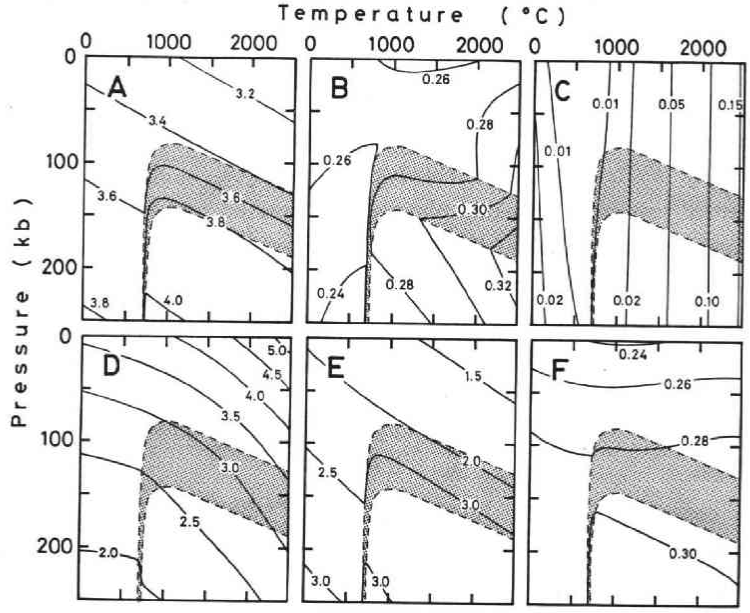

Fig. 4. Physical coefficients of mantle materials as a function of temperature and pressure. A: Density in gr/cm³. B: Specific heat at constant pressure in cal/gr·deg. C: Thermal conductivity in cal/cm·deg·sec. D: Volumetric thermal expansion coefficient in $\times 10^{-5}$/deg. E: Young's modulus in $\times 10^{12}$ dyne/cm². F: Poisson's ratio. The shaded areas represent the transition zone between 0 and 100% olivine-spinel phase change.

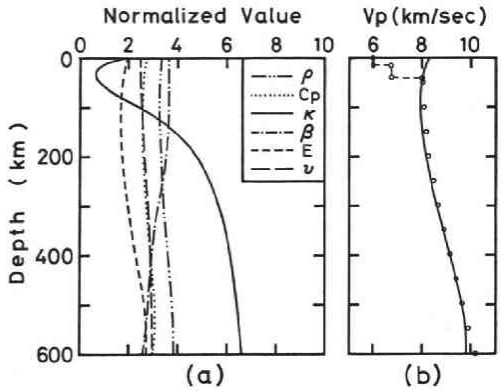

Fig. 5.

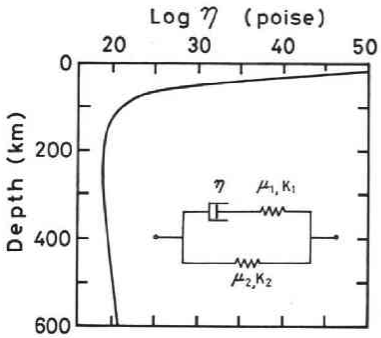

Fig. 6.

Fig. 5. Physical coefficients of mantle materials (left) and seismic velocity (right) with respect to depth. ρ: Density in gr/cm³. C_p: Specific heat at constant pressure in $\times 10^{-1}$ cal/gr·deg. κ: Thermal conductivity in $\times 10^{-2}$cal/cm·deg·sec. β: Volumetric thermal expansion coefficient in $\times 10^{-5}$/deg. E: Young's modulus in $\times 10^{-12}$ dyne/cm². ν: Poisson's ratio in $\times 10^{-1}$. The circle in the right figure is derived from the seismic velocity structure presented by Herrin (1968).

Fig. 6. Rheological model of linear standard solid for mantle materials and viscosity with respect to depth. Viscosity is derived from Sleep (1975).

temperature and pressure and, taking geotherm and pressure distribution into consideration, they are also seen in Fig. 5 versus depth.

In this study, litho- and astheno- spheres are thought to be visco-elastic bodies. The linear standard solid as represented rheologically in Fig. 6 is adopted. It is generally accepted that the asthenosphere immediately below the oceanic lithospheric plate is partially melted, and the rheological property changes considerably there. The temperature just below oceanic plate was estimated to be 1095°C and, therefore, the model is assumed to change at this critical temperature. Thus the ratio of constants K_1/K_2 and μ_1/μ_2 in Fig. 6 is assumed as 1/3 for $T \leq 1095$°C and 3.97/0.03 for $T > 1095$ °C in the present study. This implies that, when the calculated temperature exceeds 1095°C, the ratio of elastic and viscous properties are changed there.

About viscosity, the relation,

$$\eta = \frac{T}{A} \exp\left(\frac{E^* + PV^*}{RT}\right), \tag{11}$$

where R gas constant, E^* activation energy and V^* activation volume, is used. The numerical values of $E^* = 104.0$ kcal/mol, $V^* = 9.89$ cm/mol and $A = 8.70 \times 10^{-3}$ cm·sec. °K/gr are adopted according to Sleep (1975).

3. Distribution of temperature

The temperature distribution in and around descending plate thus calculated is shown in Figs. 7~10. All figures represent the temperature on the final stage of time step, which may correspond to the present stage of the earth. Fig. 7 shows temperature

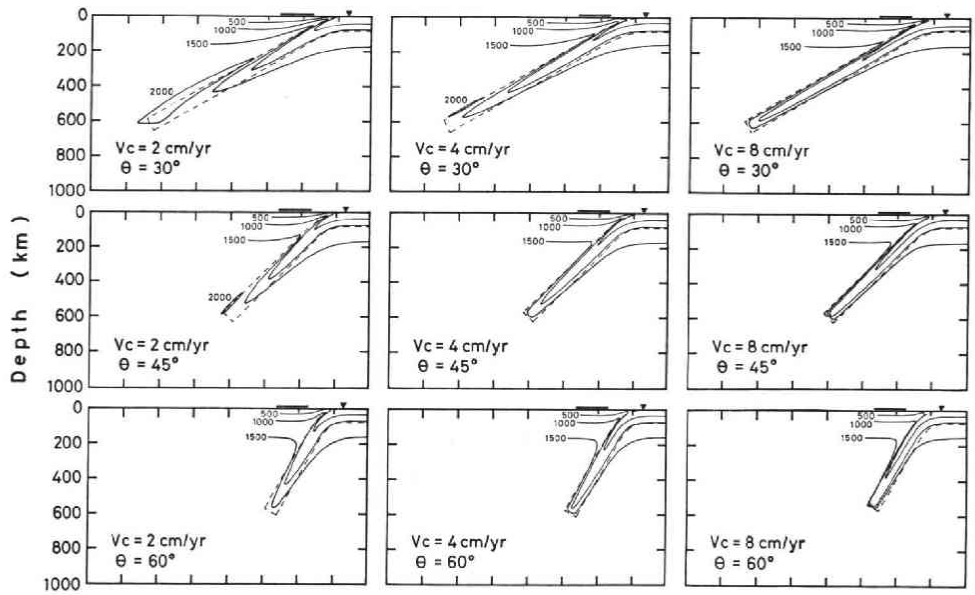

Fig. 7. Distribution of temperature in and around descending plate of the combination of Vc= 2, 4 and 8 cm/yr and θ=30, 45 and 60°. Solid lines are the iso-therm of 500, 1000, 1500 and 2000°C. The portion surrounded by the broken solid line represents the descending plate.

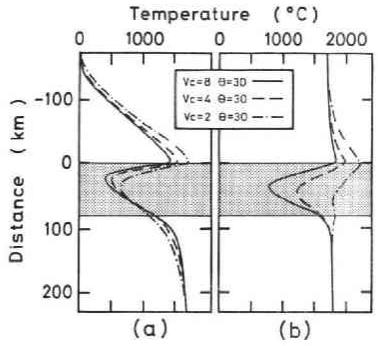

Fig. 8.

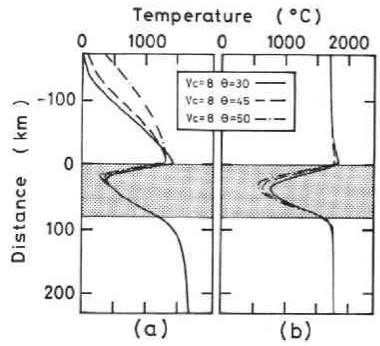

Fig. 9.

Fig. 8. Temperature profile on the cross section perpendicular to the dip of descending plate of $Vc=2$, 4 and 8 cm/yr and $\theta=30°$. The shaded area is the descending plate and the position of its center corresponds to the depth of 150 km (a) and to 500 km (b).

Fig. 9. Temperature profile on the cross section perpendicular to the dip of descending plate of $Vc=8$ cm/yr and $\theta=30$, 45 and 60°. The shaded area is the descending plate and the position of its center corresponds to the depth of 150 km (a) and to 500 km (b).

distribution for every combination of convergence velocity $Vc=2$, 4 and 8 cm/yr and dip angle $\theta=30$, 45 and 60°. Thin solid lines in the figure express the contour lines of $T=500$, 1000, 1500 and 2000°C. Broken line is the boundary between plate and surrounding asthenosphere and reverse triangle shows the location of trench. The temperature profiles on two cross sections perpendicular to dip direction in the case of $\theta=30°$ are seen in Fig. 8, the depth of center of cross sections being 150 km (a) and 500 km (b). The distance in ordinate is measured from the upper boundary of plate which is indicated by shaded portion. The temperature at center of plate with $Vc=2$ cm/yr are higher by about 200°C and 1100°C than those with 8 cm/yr for depths of 150 and 500 km respectively. This is a matter of course because the plate descending with lower velocity is heated by surrounding asthenosphere for longer time.

The dependency of temperature on dip angle is seen in Fig. 9, which expresses the temperature profile on two sections perpendicular to dip direction similarly to Fig. 8. If the dip angle is more gentle, plate should be heated for longer time till it descends to a fixed depth and the temperature should be higher as shown in Fig. 9. This figure also indicates the effect of dip angle is a little smaller than that of convergence velocity.

Another important factor which affects significantly the temperature distribution is the shear heating given at the upper boundary of descending plate. As seen in Fig. 8, the temperature at the upper boundary in the case of 2 cm/yr of velocity is about 500°C higher than that with $Vc=8$ cm/yr for the same dip angle of 30°. This is due to longer heating of plate in former case. The extreme case concerned in this study is the case of $Vc=2$ cm/yr and $\theta=30°$ shown in Fig. 7, where the region with higher temperature than 2000°C spreads along the upper boundary as widely as 300~600 km in depth.

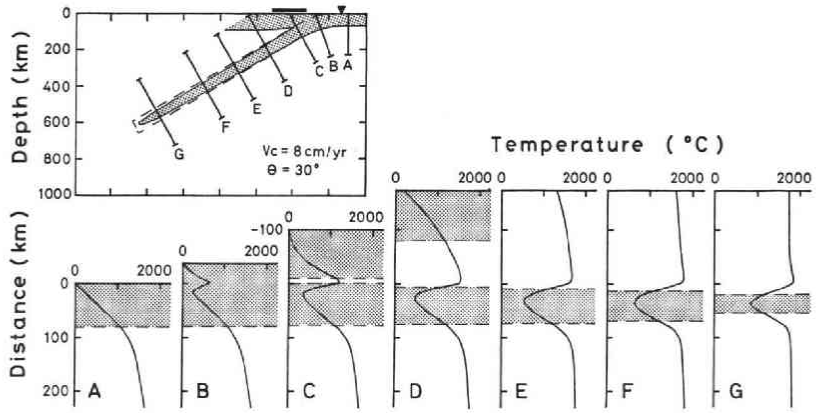

Fig. 10. Temperature profile on the cross section perpendicular to the dip of descending plate of Vc=8 cm/yr and θ=30°. Ordinate in the lower figure is the distance measured from the upper surface of plate which is surrounded by the broken line in the upper figure. Shaded areas represent the regions in which the temperature is lower than 1095°C.

The asthenosphere below plate is cooled down by plate as seen in Fig. 8 (ahe). T temperature decrease due to this effect depends on dip angle and velocity of plate. But the dependency of temperature change on velocity and dip angle is not so large as in asthenosphere above plate.

The detailed temperature distribution is shown in Fig. 10, which expresses the case of Vc=8 cm/yr and θ=30°, as an example. Lower figures show the temperature profiles on cross sections from (A) to (G) in upper figure, these sections being perpendicular to dip direction. The ordinate of lower figures in Fig. 10 represents the distance on cross section measured from the upper boundary of descending plate. The temperature variation within the plate in oceanic plate is almost linear versus depth as seen on cross section (A). As soon as the plate begins to subduct, its temperature, especially in a close area to upper surface, increases considerably as seen on (B), and the maximum of temperature rise is at a slightly lower part than the upper surface. The minimum temperature is seen at rather shallower part than the center of plate. As the cross section becomes deeper (D, E and F), the part of minimum temperature approaches to the center. Finally the temperature distribution is almost symmetric with respect to the center of plate as shown on section (G), of which the depth of center from earth's surface is about 550 km. The difference between temperature at surface of plate and the minimum value is about 750°C on section (C), the depth of center being approximately 100 km. The difference decreases with increasing depth of section.

In this study, the rheological property is taken to vary at a crticial temperature of 1095°C, as stated before. The portion of cross section, where the temperature is lower than the critical value, is represented by shaded area in figures of Fig. 10. This rather elastic portion becomes narrowes with increasing depth and the thickness is about 35 km at the depth of 550 km (section G), whereas it is 80 km on section (A).

4. Distribution of thermal stress

The non-uniform temperature distribution produces thermal stress in and around the descending plate. The calculated thermal stress is shown in Fig. 11, which represents the distribution in cases of Vc=2, 4 and 8 cm/yr and Θ=30, 45 and 60°. Solid lines in this figure are contour of maximum shear stress due to temperature distribution and the numerals represent the value of maximum shear stress in kbar. The positive in maximum shear stress implies that the maximum principal stress there is tension, while minus sign stands for compressional stress. Symbols of T and C mean the area where the maximum principal stress is tensional and compressional respectively.

It is recognized in Fig. 11 that the maximum principal thermal stress is characterized by compression and tension above 2 kbars in upper and central parts of plate, respectively. The principal axis is oriented almost parallel to dip direction. In some cases, the compressional stress is also seen in lower part of plate but its value is mostly much smaller than 2 kbars. When Vc=2 cm/yr and Θ=30°, the stress in lower part is tensional differently from other cases.

Above the descending plate the land is usually located. The location of land portion is approximately represented by a thick solid line in Fig. 11. The thermal stress distribution shown in Fig. 11 indicates that compressional part exists immediately beneath the land portion and tensional stress appears below it in most cases. However the magnitude of these stresses outside of plate is much smaller than the maximum stress within plate, which is larger than 2 kbars.

The maximum principal stress (σ_1), minimum principal stress (σ_3) and dip angle of principal axis (θ) in compressional and tensional fields are listed in Table 2, which shows

Table 2. Maximum and minimum principal stresses and dip angle of principal axis

Θ	Vc	Depth=200 km						Depth=400 km					
		Compression			Tension			Compression			Tension		
		σ_1	σ_3	θ	σ_1	σ_3	θ	σ_1	σ_3	θ	σ_1	σ_3	θ
30	2	−9.0	0.0	35	2.9	0.1	26	−2.4	0.1	36	1.2	−0.1	23
	4	−10.0	−0.1	33	3.1	−0.1	21	(−5.9	0.2	30)*	5.1	−0.3	28
	8	−14.4	0.8	32	4.1	0.1	30	−12.8	0.0	31	5.4	0.0	30
45	2	−12.4	−0.0	47	3.9	0.1	45	−10.4	0.1	48	4.1	0.1	44
	4	−14.4	0.6	47	4.0	0.1	44	−14.4	0.0	46	5.3	0.1	45
	8	−16.3	−0.0	45	3.9	0.0	46	−15.1	0.7	47	6.0	0.1	46
60	2	−14.2	0.2	61	4.1	0.2	60	−12.3	0.0	62	4.7	0.2	58
	4	−14.1	−0.0	60	3.7	0.1	60	−11.6	0.7	63	5.5	0.1	60
	8	−12.8	−0.0	60	3.5	0.1	58	−15.5	0.1	60	5.0	0.0	58

* Values at the lower part of plate.

Θ: Dip angle of descending plate in degree. Vc: Convergence velocity in cm/yr.

σ_1: Maximum principal stress in kbar. σ_3: Minimum principal stress in kbar.

Minus-sign means the compressional stress. θ: Dip angle of principal axis in degree.

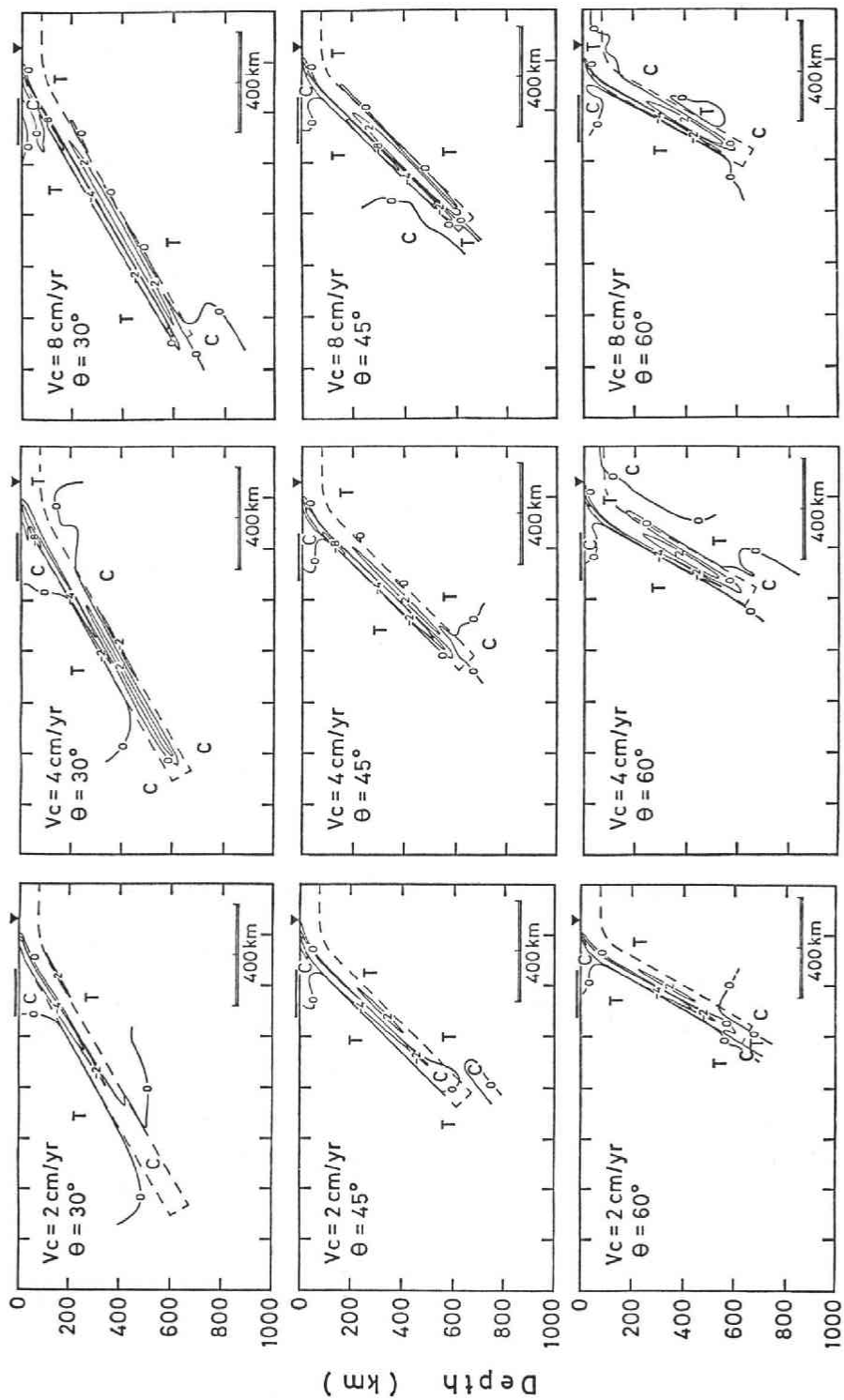

Fig. 11 (See page 95, for Figure Caption)

the values at 200 and 400 km for every case. In an exceptional case of Vc=4 cm/yr and θ=30° at 400 km in depth, the compressional stress in lower part of plate is larger than that in upper part and, therefore, the value in lower part is listed in this particular case. In other cases, the values of compression are those at the upper part of plate.

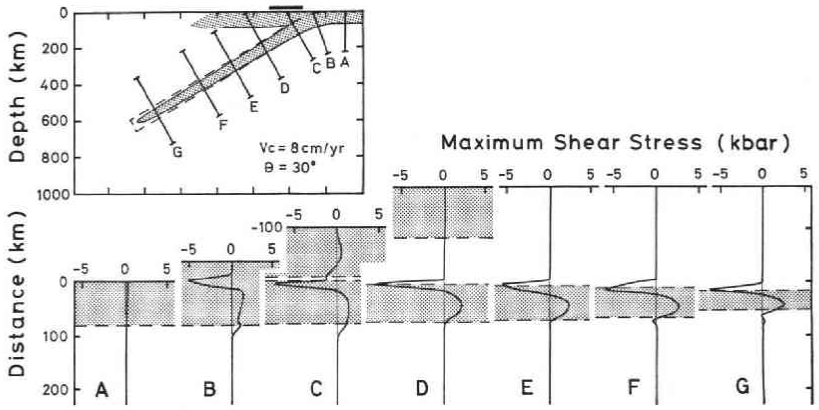

Fig. 12. Distribution of thermal stress on the cross section perpendicular to the dip of descending plate of Vc=8 cm/yr and θ=30. Ordinate in the lower figure is the distance measured from the upper surface of plate which is surrounded by the borken line in the upper figure. Shaded areas represent the regions in which the temperature is lower than 1095°C.

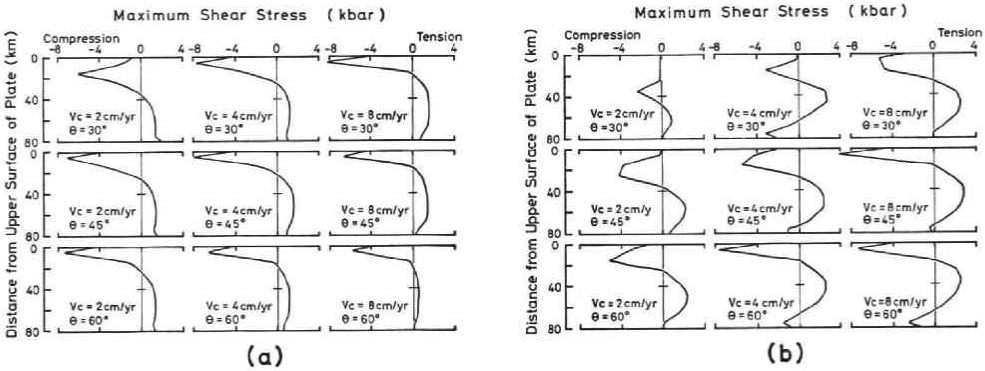

Fig. 13. Distribution of maximum shear stress of thermal stress on the cross section perpendicular to the dip of descending plate of Vc=2, 4 and 8 cm/yr and θ=30, 45 and 60°. The position at the center of plate (ordinate=40 km) corresponds to the depth of 120 km (a) and to 350 km (b).

Fig. 11. (Opposite) Distribution of thermal stress in and around descending plate of the combination of Vc=2, 4 and 8 cm/yr and θ=30, 45 and 60°. Solid lines represent the iso-maximum shear stress and the numerals indicate its magnitude in kbar, minus sign means that in which the maximum principal stress is compression. The symbols, T and C, show the tensional and compressional stress field respectively. The portion surrounded by the broken line represents the descending plate.

As seen in Fig. 11 and Table 2, the maximum principal stress in compressional field ranges from 2 to 16 kbars and the principal stress in tensional field is usually 1/2∼1/3 of that in compressional field. The dip angle of principal axis, especially in part of peak magnitude of principal stress, is parallel to that of subduction irrespective of convergence velocity and dip angle of plate.

The more detailed distributions of thermal stress on several cross sections from A∼G are seen in Fig. 12, which represents the case of Vc=8 cm/yr and θ=30° as an example. The direction of cross section is taken to be perpendicular to dip direction as shown in upper figure of Fig. 12 and the ordinate of lower figures indicates the distance along the section measured from the upper boundary of plate. The shaded part means the area where the temperature is lower than 1095°C as in Fig. 10. The thermal stress of the uppermost section (A) is almost nil irrespective of distance from upper boundary and this implies a linear change of temperature with respect to the distance. As the depth of cross section becomes larger, the temperature profile on section shows the minimum (Fig. 10) and a considerable magnitude of thermal stress is produced. Compressional stress more than 5 kbars is seen in the upper part of plate and tensional stress more than 2 kbars appears in central part. When the depth reaches 100 and 200 km (C and D), the stress shows maximum magnitude because the difference in temperature between upper and central parts is largest. For cross sections deeper than 200 km (E, F and G), the stress decreases gradually. The areas where compressional and tensional stresses are larger than 5 and 2 kbars respectively are located almost parallel to dip direction on every section. Fig. 12 also implies that the distance between peaks of compressional and tensional stresses decreases with increasing depth. Actually this distance is about 40 km on sections (C) and (D) and it becomes 30 km on section (G), which corresponds to 550 km in depth.

Fig. 12 indicates the thermal stresses on deep sections (D, E, F and G) are very small outside of plate. The temperature in this area is higher than 1095°C as seen in Fig. 10 and the thermal stress is relaxed by the viscous property of material. In upper area (C), where the temperature is not so high, the thermal stress of about 1 kbars is seen.

The qualitative features of thermal stress are similar in every cases, although Fig. 12 represents a particular case of Vc=8 cm/yr and θ=30°. The quantitative dependency of stress on Vc and θ is seen in Figs. 13, 14 and Table 3. Fig. 13 shows the stress distribution in various cases of Vc and θ on cross section similarly to Fig. 12, Fig. 13 (a) and (b) corresponding to sections of which the centers are located at 120 and 350 km in depth. Horizontal axes stand for maximum shear stress in kbar with plus and minus signs for tension and compression respectively. Vertical axis represents the distance from upper boundary of plate. It is seen in Fig. 13 that the stress pattern is qualitatively similar irrespective of Vc and θ, as stated above, although the location of stress peak varies considerably with respect to Vc and θ. For example, as seen in Fig. 13(b), the peak of compressional stress appears at about 5, 15 and 35 km from the upper surface of plate when Vc is 8, 4 and 2 cm/yr respectively for θ=30°. The location

of stress peak mentioned above is close to the region where temperature is 1095°C. Therefore, if the part of lower temperature than 1095°C is taken to be the "real" plate, it may be said that the peak of stress exists very close to the upper boundary of "real" plate.

The distance between peaks of compressional and tensional stress at 300 km in depth (Fig. 13b) becomes closer as V_c approaches to 2 cm/yr but such a tendency is not clear at the depth of 120 km (Fig. 13a). The dependency of the distance between peaks upon dip angle is not so evident either.

Table 3 represents the maximum values of maximum shear stress in compressional and tensional fields at 200 and 400 km in depth for various convergence velocities and dip angles, this being illustrated also in Fig. 14. The compressional and tensional

Table 3. Maximum shear stress versus convergence velocity and dip angle of plate

Dip Angle	Depth=200 km			Depth=400 km		
	Convergence Velocity (cm/yr)					
	2	4	8	2	4	8
	Compression			Compression		
30°	4.5	5.0	7.6	1.3	3.0*	6.4
45°	6.2	7.5	8.2	5.3	7.2	7.9
60°	7.2	7.0	6.4	6.2	6.1	7.8
	Tension			Tension		
30°	1.4	1.6	2.0	0.7	2.7	2.7
45°	1.9	2.0	1.9	2.0	2.6	3.0
60°	2.0	1.8	1.7	2.3	2.7	2.5

* Value at the lower part of plate.

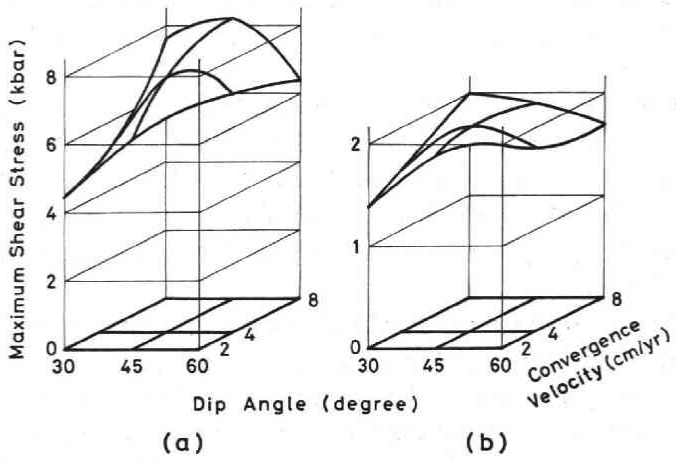

Fig. 14. Dependency of magnitude of thermal stress on convergence velocity and dip angle. (a) is in compressional stress field and (b) is in tensional stress filed, respectively, at 200 km in depth.

fields usually appear in the upper and central parts of plate respectively, except for the case of V_c=4 cm/yr and θ=30° at 400 km deep.

As seen in Fig. 14 and Table 3, the dependency of maximum stress on Vc and θ is not so simple. In compressional field at 200 km in depth, for fixed angles of θ=30° and 45°, the maximum stress increases with increasing velocity, while, at θ=60°, it decreases with increasing velocity. For a fixed Vc of 2 cm/yr, it increases with increasing θ, while, for Vc=4 and 8 cm/yr, it shows a maximum at θ=45°. Similar characteristics of maximum stress is also the case of compressional field at 400 km and tensional fields at 200 and 400 km. It is natural that the value of maximum stress is smallest when Vc=2 cm/yr and θ=30°, because the uniformity of temperature distribution within plate is reasonably accepted in this case compared to other cases as stated in the former section.

It is very interesting that the largest values of both compressional and tensional stresses are obtained for Vc=8 cm/yr and θ=30 or 45°, which correspond to the situation in Northeastern Honshu, Japan where is one of the most typical subduction zone and where the double-planed seismicity of intermediate focus earthquakes is extremely clear.

5. Considerations on effects of various assumptions

The distribution of thermal stress in and around the descedning plate described in the previous section is calculated under several assumptions and the effects of these assumptions on results is discussed in this section.

5.1. Effects of boundary conditions

The result explained in section 4 are calculated under the condition that the displacement is free along boundaries of region in concern, say on the surface of A~B~C~D~E~F~A in Fig. 3. This assumption does not cause so serious effect, because the calculated displacement on these surfaces is small even under the assumption of free displacement.

There are two other boundary conditions which should be taken into account. One is that on the upper surface of plate and the other is that at the bottom tip of plate. To examine of effects by these conditions, the calculation is made for a simpler model than that adopted so far. Distributions of temperature and thermal stress within plate is estimated giving boundary conditions on its surface without consideration for outside part of plate.

The fault plane of large earthquake of thrust type sometimes located at the boundary between descending plate and continental lithosphere. If this kind of event is a result of stick-slip fracture, this boundary should be fixed. To examine the effect of boundary condition there, calculations of thermal stress as well as temperature are made using the simplified model (see Goto and Hamaguchi, 1983) for the cases where free displacement is allowed on the whole surface of upper boundary of plate and where zero displacement is assumed at the part of boundary above 50 km in depth.

Although the numerical result is not shown here, the compressional stress field in the latter case expands to some extent in comparison with the former case but the difference between two cases is so small for the plate below 70 km. Therefore, it is concluded that the boundary condition between descending plate and continental lithosphere does not cause any essential influence as far as the intermediate deep focus earthquakes are concerned.

On the other hand, the boundary condition at the bottom of plate is very influential. Some investigators (e.g. Isacks and Molnar, 1971; Sleep, 1979) thought that the bottom tip of plate contacts directly with mesosphere and others claimed that the plate is not contact with mesosphere because of assimilation of plate with surrounding asthenospher around the bottom tip. In the former case, if mesosphere is rigid, the tip should be fixed, whereas, in the latter case, free displacement condition at bottom tip may represent the situation. In order to examine which is better, thermal stress in both cases is calculated using the simplified model and the result is shown in Fig. 15 for $Vc=8$ cm/yr and $\theta=30°$ as an example. Solid lines in this figure are contours of maximum shear stress, of which the values in kbar being expressed by numerals aside of them. Shaded area is the region where the maximum principal stress is tension. It should be noted that the distribution of thermal stress is quite similar to that in Fig. 11 in the case (A), where free displacement condition is given at the tip, and it implies the validity of adopted of simplified model. The distribution of thermal stress in Fig. 15(B), which represents the case of fixed condition at the tip, is much different from that in case (A). The description of this discrepancy was made in more detail in another paper by Goto and Hamaguchi (1983). Simply speaking, however, the whole plate shows the field of compressional stress, the maximum shear stress being 10 and 2 kbars at upper and central part respectively. It may be said, in other words, that if a constant compression, say 5 kbars, is added to the distribution in Fig. 15(A), it should roughly represents that in Fig. 15 (B). Therefore, the intermediate state between (A) and (B) is inferred to show a distribution composed of summation of that in

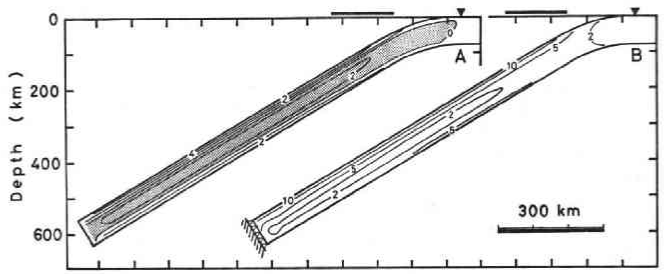

Fig. 15. Distribution of thermal stress in the descending plate of $Vc=8$ cm/yr and $\theta=30°$ estimated under the condition that the displacement at the boundaries is free (A) and the condition that the displacement at the bottom tip of plate is fixed completely (B). Solid lines represent the iso-maximum shear stress and numeral is its magnitude in kbar. Shaded area means in which the maximum principal stress is tension. The results in this figure are based on the calculation in considering only the descending plate and its treatment is stated in detail in Goto and Hamaguchi (1983).

Fig. 15 (A) and a compressional stress with constant value less than 5 kbars. In any case, case (A) is concluded to be better than case (B) when the characteristics of observed double-planed seismic zone under typical island arc is taken into account. It is a very important conclusion in considering the state of descending plate that the free displacement can explain better the actual seismicity than the assumption of fixed tip.

5.2. *Effect of shear heating*

In the present calculation, constant rate of shear heating of 1.5×10^{-11} cal/cm^3·sec is assumed along the upper boundary of plate. Now the discussion is made on how much change in thermal stress is produced by different constant value and how is the dependency of the change on Vc and θ. For the examination the distributions of temperature and thermal stress with no shear heating are calculated using the same model and their profiles on the cross section with the depth of 200 km at its center are shown in Fig. 16, which represents the case of $Vc=8$ cm/yr and $\theta=30°$. The corresponding profile when shear heating of 1.5×10^{-11} cal/cm^3·sec is given is also indicated in the figure for comparison.

The difference in temperature between two cases is prominent in the area of about 80 km above and 50 km below the upper boundary of plate and maximum difference amounts to 600°C and 100°C around upper and central parts of plate respectively. The corresponding difference in thermal stress naturally appears in the same area, the difference in maximum shear stress being shown in Fig. 16. When no shear heating is given, the tensional stress of 4 kbars is seen immediately above the boundry, while almost no stress exists there when shear heating is applied. This situation is reasonably understood by considering that, if shear heating does not exist, asthenosphere outside of plate

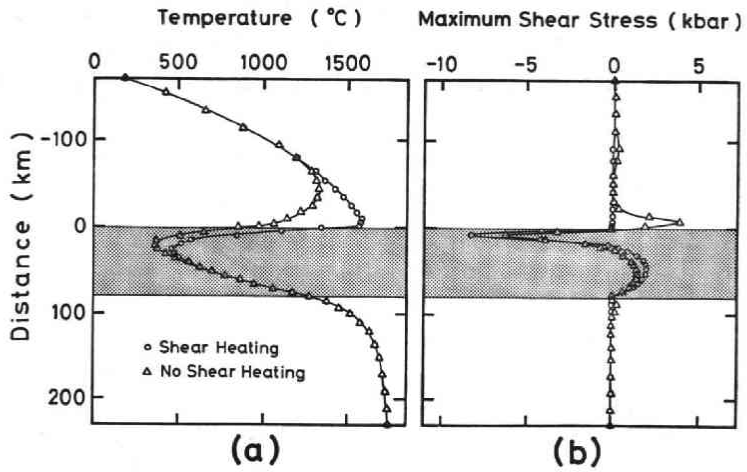

Fig. 16. Distributions of temperature (a) and of thermal stress (b) on the cross section perpendicular to the dip of descending plate of $Vc=8$ cm/yr and $\theta=30°$. The position at the center of plate (shaded area) corresponds to the depth of 200 km. The circle represents the result obtained by considering the shear heating of 1.5×10^{-11} cal/cm^3·sec and triangle is that obtained by considering no shear heating.

should be cooled by colder plate at least in a close area to boundary and the contraction due to the cooling causes tensional stress.

The difference in stress within plate is relatively small and a slight decrease in stress is seen in the case of no shear heating compared to the case with shear heating. This is due to the circumstance that the difference in temperature in the plate is smaller when no shear heating is applied.

The dependency of stress difference on V_c and Θ is a little complicated. The rise of temperature around plate boundary by shear heating is reasonably larger for slower convergence velocity and lower dip angle. However, when the temperature is higher than a critical temperature, which is assumed to be 1095°C in the present study, the effect of viscosity releases the stress induced the temperature difference. For an example, this stress release occurs almost completely at about 350 km in depth in the case of $Vc=2$ cm/yr and $\Theta=30°$. Although the quantitative discussion on this point is not enough here, it may be eventually concluded that the dependency of stress distribution on V_c and Θ is not so strong.

5.3. Effect of physical properties of material

In the present study, the dependency of physical properties of material on temperature and pressure is assumed as described in section 2. The relations between the properties and temperature or pressure, however, have not been established with a satisfactory accuracy and it is necessary to check the effect of the ambiguity on obtained results. Fig. 5 implies that, among various factors, thermal conductivity may be most influential in this problem. For the examination of the effect in concern, therefore, the distribution of temperature is calculated for a constant conductivity of 0.01 cal/cm·deg·sec, keeping other factors as they are. The comparison of two cases of temperature and pressure

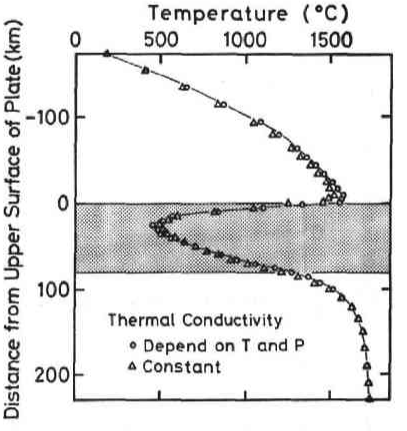

Fig. 17. Distribution of temperature on the cross section perpendicular to the dip of descending plate of $Vc=8$ cm/yr and $\Theta=30°$. The position at the center of plate (shaded area) corresponds to the depth of 200 km. The circle represents the temperature obtained by considering the dependency of thermal conductivity on temperature and pressure and the triangle is that obtained by considering the constant thermal conductivity of 0.01 cal/cm·deg·sec.

dependent and independent conductivity is seen in Fig. 17, which represents the temperature profile on a cross section of 200 km depth at its center. Since the difference in temperature between two cases is as small as 80°C or less, the effect of change in thermal conductivity, as well as other factors concerning physical properties of material, is concluded to be negligibly small.

5.4. Effect of interaction between plate and asthenosphere

The present calculation is carried out in the region shown in Fig. 3 as one block without any boundary condition at the surface of descending plate. This implies that the plate has a completely cohesive interaction with surrounding asthenosphere. To examine the effect of coherency, thermal stress is estimated in another extreme case where the boundary condition of free displacement on the surface of plate is given, assuming the same distributotion of temperature as in the present calculation. Then the force balance should be made only within plate. This condition corresponds to the case of no interaction between plate and asthenosphere. Several studies (e.g. House Jacob, 1982) have been carried out under such a condition. The comparison of results for both conditions is shown in Fig. 18, which represents profiles of thermal stress on a cross section with the depth of 200 km for Vc=8 cm/yr and Θ=30°. As seen in this figure, considerable differences are seen between two cases. In the particular case shown in Fig. 18, 2.5~3 kbars of stress difference is obtained at the upper and central parts of plate and, furthermore, the large compressional stress amounting to about 8.5 kbars is found at the lower part.

The condition adopted in the present study, which takes the existence of asthenosphere outside of plate into acount, may be thought to be advantages from two view points compared to the case of free interaction between plate and asthenosphere. First

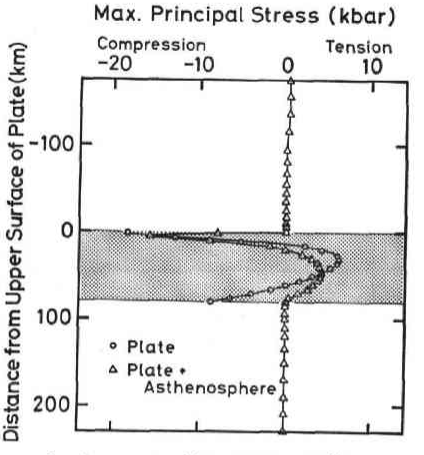

Fig. 18. Distribution of thermal stress on the cross section perpendicular to the dip of descending plate of Vc=8 cm/yr and Θ=30°. The position at the center of plate (shaded area) corresponds to the depth of 200 km. The circle represents the stress in no interaction between the descending plate and asthenosphere and the triangle is that in completely cohesive interaction of them as presented so far.

is that some interaction should natually exist in actual case and that it may be reasonable to consider that the real interaction is rather closer to complete coherence than zero. Secondly the assumption of free interaction, which results in a high compressional stress in lower part of plate, cannot explain the observed aseismicity there.

6. Summarized conclusions

In the present part of this study, thermal stress in and around descending plate is estimated by FEM for plates with convergence velocity (Vc) of 2, 4 and 8 cm/yr and dip angle (θ) of 30, 45 and 60°, taking the dependency of physical properties of material on temperature and pressure into acount. The influence of adopted assumptions on the obtained results are examined. The main conclusions in this part are as follows:

(1) The stress pattern is characterized by compressional and tensional stresses at the upper and central parts of plate respectively, principal axes being oriented almost parallel to dip direction.

(2) The magnitude of maximum shear stress depends strongly on Vc and θ and, in some case, it reaches to about 8 and 3 kbars in compressional and tensional fields respectively.

(3) The maximum stress reveals high value at high Vc and small θ in general, although its relation to Vc and θ is not simple.

(4) The condition at the bottom tip of plate is most essential among various boundary conditions and it is proved that the condition of free displacement at the tip can explain actual seismicity better than that of fixed tip.

(5) The assumption on shear heating along the upper surface of plate causes essential effect on stress distribution for the part close to the surface.

(6) The effect of assumption on physical properties of material is revealed to be negligibly small.

(7) It is essential for the explanation of aseismic region in lower part of plate that the existence of asthenosphere surrounding plate is taken into account.

Stresses within descending plate due to other causes, as well as the comparison with thermal stress, will be described in later part of this study.

(to be continued)

References

Akimoto, S., M. Akaogi, K. Kawada and O. Nishizawa, 1976: Mineralogic distribution of iron in the upper half of the transition zone in the earth's mantle, Amer. Geophys. Union, geophys. Monogr., **19**, 399–405.

Billington, S., 1980: The morphology and tectonics of the subducted lithosphere in the Tonga-Fiji-Kermadec region from seismicity and focal mechanism solutions, Ph. D. thesis, University of Cornell.

Chung, D.H., 1971: Elasticity and equations of state of olivines in the Mg_2SiO_4-Fe_2SiO_4 system, Geophys. J.R. astr. Soc., **25**, 511–538.

Elsasser, W.H., 1969: Convection and stress propagation in the upper mantle, In: The

application of modern physics to the earth and planetary interiors (ed., S.K. Runcorn), Wiley-interscience, New York, 223–246.

Engdahl, E.R. and C.H. Scholz, 1977: A double Benioff zone beneath the central Aleutians: An unbending of the lithosphere, Geophys. Res. Lett., **4**, 473–476.

Goto, K. and H. Hamaguchi, 1983: Characteristics of distribution of thermal stress and stress due to phase change in descending plate beneath island arc, Zisin (J. Seism. Soc. Japan), Ser. II, **36**, 31–41 (in Japanese with English abstract).

Goto, K., H. Hamaguchi and Z. Suzuki, 1983: Distribution of stress in descending plate in special reference to intermediate and deep focus earthquakes, II. Characteristics of distribution of stress due to olivine-spinel phase change, in preparation.

Hamaguchi, H., K. Goto and Z. Suzuki, 1983: On the double-planed structure of intermediate-depth seismic zone beneath the Northeastern Japan, in preparation.

Hamaguchi, H., K. Goto and Y. Wada, 1977: Icequakes observed in the Lake Suwa, (3) Relationship between icequakes and temperatures, abstract presented at the spring meeting of Seism. Soc. Japan, **127** (in Japanese).

Hasegawa, A., N. Umino and A. Takagi, 1978a: Double-planed structure of the deep seismic zone in the Northeastern Japan arc, Tectonophysics, **47**, 43–58.

Hasegawa, A., N. Umino and A. Takagi, 1978b: Double-planed seismic zone and upper mantle structure in the Northeastern Japan arc, Geophys. J.R. astr. Soc., **54**, 281–296.

Herrin, E., 1968: Introduction to "1968 Seismological Tables for P phases", Bull. Seism. Soc. Amer., **58**, 1193–1241.

Horii, K. and M. Kawahara, 1970: A numerical analysis on visco-elastic structures by the finite element method, Proc. Japan Soc. C. Engin., **179**, 23–35.

House, L.S. and K.H. Jacob, 1982: Thermal stresses in subducting lithosphere can explain double seismic zones, Nature, **295**, 587–589.

Iriyama, J., 1966: On the thermal history of the earth, Zisin (J. Seism. Soc. Japan), Ser. II, **19**, 11–22 (in Japanese with English abstract).

Isacks, B. and P. Molnar, 1971: Distribution of stresses in the descending lithosphere from a global survey of focal-mechanism solutions of mantle earthquakes, Rev. Geophys. Space Phys., **9**, 103–174.

Kasahara, K., M. Ohtake and K. Iida, 1979: Microearthquake activity in the Kanto district, abstract presented at the autumn meeting of Seism. Soc. Japan, 49 (in Japanese).

Kingery, W.D., J. Francl, R.L. Coble and T. Vasilos, 1954: Thermal conductivity: (10) Data for several pure oxide materials corrected to zero porosity, J. Amer. Ceramic Soc., **37**, 107–110.

Linde, A.T. and I.S. Sacks, 1978: On double Benioff zones in subduction regions, Carnegie Inst. Wash. Year Book **77**, 517–520.

Lubimova, E.A., 1967: Theory of thermal state of the earth's mantle, In: The earth's mantle (ed., T.F. Gaskell), Academic Press, London and New York, 232–323.

McKenzie, D.P., 1967: Some remarks on heat flow and gravity anomalies, J. Geophys. Res., **72**, 6261–6273.

Minear, J.W. and M.N. Toksöz, 1970: Thermal regime of downgoing slab, Tectonophysics, **10**, 367–390.

Neugebauer, H.J. and B. Breitmayer, 1975: Dominant creep mechanism and the descending lithosphere, Geophys. J.R. astr. Soc., **43**, 873–895.

Okada, H., 1971: Forerunners of ScS wave from nearby deep earthquakes and upper mantle structure in Hokkaido, Zisin (J. Seism. Soc. Japan), Ser. II, **24**, 228–239 (in Japanese with English abstract).

Pascal, G., B.L. Isacks, M. Barazangi and J. Dubois, 1978: Precise relocations of earthquakes and seismotectonics of New Hebrides island arc, J. Geophys. Res., **83**, 4957–4973.

Reyners, M. and K.S. Coles, 1982: Fine structure of the dipping seismic zone and subduction mechanics in the Shumagin Islands, Alaska, J. Geophys. Res., **87**, 356–366.

Ringwood, A.E., 1970: The system Mg_2SiO_4-Fe_2SiO_4 at high pressures and temperatures, Phys. Earth Planet. Interiors, **3**, 89–108.

Ringwood, A.E., 1972: Mineralogy of the deep mantle: Current status and future developments, In: The nature of the solid earth (ed., E.C. Robertson), McGraw-Hill, New York, 67–92.

Samowitz, I.R. and D.W. Forsyth, 1981: Double seismic zone beneath the Mariana island arc, J. Geophys. Res., **86**, 7013–7021.

Sawamoto, H., 1977: Orthorhombic perovskite (Mg, Fe)SiO_4 and constitution of the lower mantle, In: High-pressure research (eds., M.N. Manghnani and S. Akimoto), Academic Press, New York, 219–244.

Sleep, N.H., 1975: Stress and flow beneath island arcs, Geophys. J.R. astr. Soc., **42**, 827–857.

Sleep, N.H., 1979: The double seismic zone in downgoing slabs and the viscosity of the mesosphere, J. Geophys. Res., **84**, 4565–4571.

Smith, A.T. and M.N. Toksöz, 1972: Stress distribution beneath island arcs, Geophys. J.R. astr. Soc., **29**, 289–318.

Sumino, Y., O. Nishizawa, T. Goto, I. Ohno and M. Ozima, 1977: Temperature variation of elastic constants of single-crystal forsterite between −190° and 400°C, J. Phys. Earth, **25**, 377–392.

Sung, C.M. and R.G. Burns, 1976: Kinetics of high-pressure phase transformations: Implications to the evolution of the olivine→spinel transition in the downgoing lithosphere and its consequences on the dynamics of the mantle, Tectonophysics, **31**, 1–32.

Suzuki, I., 1975: Thermal expansion of periclase and olivine, and their anharmonic properties, J. Phys. Earth, **23**, 145–159.

Suzuki, I., E. Ohtani and M. Kumazawa, 1980: Thermal expansion of modified spinel, β-Mg_2SiO_4, J. Phys. Earth, **28**, 273–280.

Suzuki, S. and Y. Motoya, 1981: Microearthquake activity in Hokkaido observed by the telemetering system, Zisin (J. Seism. Soc. Japan), Ser. II, **34**, 251–267 (in Japanese with English abstract).

Suzuki, M., N. Umino, A. Hasegawa and A. Takagi, 1980: Microearthquake activity in Northern Kanto and Southern Tohoku, Japan, abstract presented at the autumn meeting of Seism. Soc. Japan, 64 (in Japanese).

Toksöz, M.N., N.H. Sleep and A.T. Smith, 1973: Evolution of the descending lithosphere and the mechanisms of deep focus earthquakes, Geophys. J.R. astr. Soc., **35**, 285–310.

Tsukahara, H., 1980: Physical conditions for double seismic planes of the deep seismic zone, J. Phys. Earth, **28**, 1–15.

Tsumura, K., 1973: Microearthquake activity in the Kanto district, Publication for the 50th anniversary of the Great Kanto Earthquake, 1923, 67–87 (in Japanese with English abstract).

Tsumura, K. and T. Karakama, 1981: Deep seismic plane in Kanto district, Japan, abstract presented at the autumn meeting of Seism. Soc. Japan, 8 (in Japanese).

Umino, N. and A. Hasegawa, 1975: On the two-layered structure of deep seismic plane in Northeastern Japan arc, Zisin (J. Seism. Soc. Japan), Ser. II, **28**, 125–139 (in Japanese wish English abstract).

Veith, K.F., 1974: The relationship of island arc seismicity to plate tectonics, Ph. D. thesis, Southern Methodist University, Dallas, Texas.

Von Herzen, R.P., 1967: Heat flow and some implications for the mantle, In: The earth's mantle (ed., T.F. Gaskell), Academic Press, London and New York, 197–230.

Yang, M., M.N. Toksoz and A.T. Smith, 1977: Thermoelastic analysis of the stresses in a subduction region, (abstract), EOS, Trans. Amer. Geophys. Union, **58**, 1233.

Yoshii, T., 1973: Upper mantle structure beneath the North Pacific and the marginal seas, J. Phys. Earth, **21**, 313–328.